2014 IEEE International Conference on Robotics & Automation (ICRA)
Hong Kong Convention and Exhibition Center
May 31 - June 7, 2014. Hong Kong, China

Dynamic effects of Asymmetric In-Phase Flapping (AIF) on forward flight

Joon-Hyuk Park, *Student Member, IEEE* and Sunil K. Agrawal, *Member, IEEE*
Robotics and Rehabilitation (ROAR) Laboratory, Mechanical Engg., Columbia University, New York, NY 10027
{jp3350 and sunil.agrawal}@columbia.edu

***Abstract*— This paper presents computational and experimental analyses on flight dynamics of Flapping Micro Air Vehicles (FWMAV) employing a novel flapping mechanism, denoted as AIFM (Asymmetric In-phase Flapping Mechanism). This mechanism was designed to achieve controlled, asymmetric in-phase wing flapping inspired by nature's flyers. This paper extends our previous study where modeling and optimization of such a mechanism was carried out. The dynamic effects of asymmetric in-phase flapping motion during forward flight are our main focus in this study. Kinematics and rigid body dynamics modeling are first carried out to derive the equations of motion of the system, followed by aerodynamic modeling of wing using blade element theory and quasi-unsteady analysis techniques. The analysis deals with three configurations of the system: symmetric in-phase flapping motion (c_0) versus asymmetric in-phase flapping motion (c_{+5}, c_{-5}). Scaled model of AIFM was fabricated and implemented into a FWMAV to show its practical feasibility. Some of the key dynamic effects of AIFM are addressed, suggesting AIFM solely can generate aerodynamic forces and moments which have the potential to bring higher agility and controllability to existing FWMAV platforms.**

Nomenclature

q_i	joint angle
l_i	link length
l_{ic}	center of mass of link i
m_i	link mass
I_i	moment of inertia of link i
r_i	span length from root to the ith strip of wing
b	total span length (mm)
β_0	coefficient of the dynamic twist (degree/m)
θ_a	pitch angle of flapping axis with respect to U
θ_w	mean pitch angle of chord with respect to flapping axis
$\delta\theta$	dynamically varying pitch angle $[= \beta_0 r_i \cos(q_1)]$
θ_t	pitch angle of the chord relative to U
C_{df}	drag coefficient due to skin friction
V_x	flow speed tangential to the section
Re	Reynolds number
Φ	flapping amplitude
f	flapping frequency (Hz)
U	flight speed (m/s)
ρ	atmospheric density (kg/m^3)
v	kinematic viscosity (m^2/s)

I. Introduction

We have witnessed remarkable advancements in Flapping Wing Micro Air Vehicle (FWMAV) technology in terms of downsizing to insect scale and realizing more complex wing motion capabilities. However, there still remain unexplored areas such as differentially varying the patterns of two flapping wings or actively altering the center of mass location. Therefore, the level of agility and maneuverability of current FWMAV technology, not to mention the flight efficiency, is still behind what we observe in nature. For typical Penaud-type FWMAV utilize a single or double crank and symmetrically placed double rockers (Fig. 1) to flap two wings symmetrically in order to attain equivalent lift and thrust generation from both wings, while flight controls are generally achieved through rudder and elevator control commonly placed on the tail.

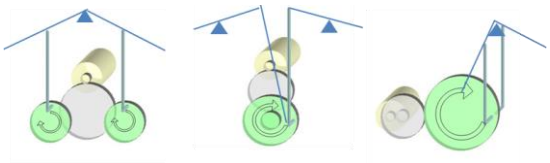

Figure 1. Examples of crank-rocker mechanisms commonly used in FWMAV to generate a flapping motion. Symmetric motion is desired between two rockers as it directly affects to the stability of FWMAV

The inner portions of the wings are inclined at a positive angle of attack and generate lift similar to airplane wings while the tip portions of the wings act as a propeller and generate thrust as illustrated in Fig. 2. In this way, the flight can be stabilized and easily controlled by means of aircraft-like tail. In this regard, the FWMAV is not able to successfully perform high maneuvers as seen in nature's flyers since it still banks, turns and climbs in a manner very similar to fixed wing aircrafts. The flight stability of this type of FWMAV, therefore, highly depends upon symmetric motion of the two wings. Slight difference in flapping amplitude or phase between the two wings often results in inherent rolling or yawing behavior which requires biasing the tail control surface to attain a stable flight.

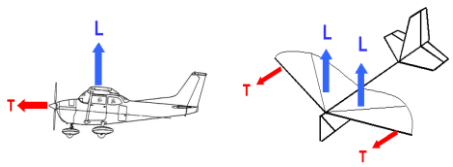

Figure 2. In airplanes, propellers generate thrust and wings produce lift. In typical penaud-type FWMAVs, lift is produced from the inside portions of the wings while the portions near the tips generate thrust

The motivation of this research comes from the observed instability in FWMAV induced by asymmetry between two wings. Our goal is to identify the dynamic effects of such asymmetric flapping on forward flight. Furthermore, present work is based on using Asymmetric In-phase Flapping Mechanism (AIFM) developed in our previous study [1]. Before getting into detail on this mechanism, reviewing the following phenomena in insect's flight will be helpful to rationalize the purpose of this study. The high speed video capturing tethered flight of *Coleoptera* (beetle) shows the asymmetric in-phase flapping feature exhibited in insects (Fig. 3). It is observed that beetle flies in a circle while tethered, two wings flap with different amplitudes but in-phase, i.e., the instances of completing upstroke and downstroke of two wings are the same but only the amplitude varies. It was reported that this actuation uses direct muscles in thorax to modulate asymmetric lift generation from each wing thereby generating a yaw motion [4].

Figure 3. Tethered flight of a *Coleoptera* showing asymmetric in-phase wing flapping

There are a number of studies which have investigated the aspect of asymmetric flapping motion in body torque generation and how it can help achieve high maneuverability and stability during flight. To turn, insects asymmetrically modulate the wing amplitude of each wing to generate asymmetric rowing motions [2]. Only a slight actuation that biases their wing motion can generate high maneuvers [3]. It was also reported that the asymmetric aerodynamic forces can provide a torque to counteract the body rotation [5, 6]. Few studies address such asymmetry in wing stroke amplitudes in FWMAV [7, 8]. The motion was typically generated by piezoelectric actuators and flexible composites where in-phase feature may not be precisely controlled. Also, a piezoelectric actuator based FWMAV generally needs to be tethered for power transmission which brings some limitations for field application.

This paper begins with describing an AIFM model which can asymmetrically modulate two wing's flapping amplitudes while guaranteeing in-phase flapping motion. Next, the formulation of kinematic and dynamic equations, followed by aerodynamic modeling of a wing is presented. The dynamic effects of AIFM on forward flapping flight are investigated through computational simulation and simulated results are partially verified experimentally using a physical construction of the mechanism.

II. Kinematics and Rigid Body Dynamics

A. Mechanism detail

The AIFM consists of two planar four bar mechanisms comprising a gearbox, and two Revolute-Revolute-Prismatic -Revolute (RRPR) mechanisms, all of which are driven by a single crank OA. The idea is to add additional shell to the aforementioned gearbox and modulate gearbox's lateral position inside a shell to achieve different wing outputs. The motor drives crank OA, which drives two couplers (AB_L and AB_R). Each coupler is then connected to a rocker, B_RD_R and B_LD_L, respectively. Rockers are pivoted at points C_R and C_L inside the gearbox, shown as a box in Fig. 4. Then the gearbox can slide laterally through the line E_RE_L. Two RRPR mechanisms ($C_RD_RE_R$ and $C_LD_LE_L$), each connects the rocker output (BC) to wing output (EF) by having R joint at C_R(C_L), RP joints at D_R(D_L) and another R joint at E_R(E_L). E_R and E_L are fixed points on the external frame, depicted as "shell". When gearbox shifts laterally, the distance between the gearbox and the shell (i.e., C_RE_R and C_LE_L) changes which brings about asymmetry in wing output. In this process, only the amplitude of two wings' output can be varied without affecting the in-phase feature of the two wings.

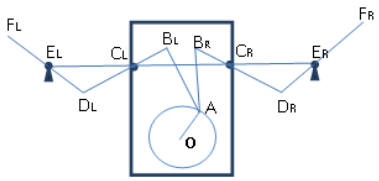

Figure 4. schematic drawing of the mechanism: i) double four bar mechanism (gearbox) generates symmetric, in-phase output to rockers ii) RRPR mechanism translates gear box output to wings iii) lateral shifting mechanism translates gearbox laterally inside the outer shell to create asymmetry between two wing outputs

It is a single degree-of-freedom mechanism if we consider the lateral shifting mechanism as a constant input parameter. The salient feature of this mechanism is that adding one more degree-of-freedom to the common double-four bar flapping mechanism, one can achieve asymmetric in-phase flapping motion of wings. The kinematics of the wings was evaluated through simulation and the simulation results were verified experimentally. Both the simulation and experiment results showed that the in-phase feature was maintained for both the symmetric and asymmetric cases (see [1] for details).

B. Kinematics

The joint kinematics can be derived from graphical approach using vector loop closure of sub-mechanisms. Since it was considered as one degree-of-freedom mechanism with single crank input angle q_1, rest of joint angles (i.e., $q_2 \sim q_7$ shown in Fig 5) can be expressed as a function of q_1. The derivation of kinematics will not be discussed here, but can be found in [1].

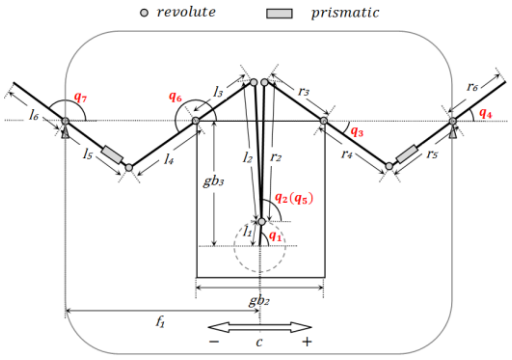

Figure 5. Schematics of AIFM.

C. Rigid body dynamics

Once all the joint angle expressions are derived, the equations of motion of a system can be obtained by first expressing the kinetic energy (K_i) and the potential energy (V_i) of sub-chains; crank-coupler chain (l_1 to l_2), rocker to ext. rocker chain (l_3 to l_4), wing-arm chain (l_5 to l_6). The length of each component is shown in Table I. Note that the same value is used for both right and left components ($r_i = l_i$). The mass of each component was determined from the physical model which will be shown in section IV.

TABLE I. LENGTH AND MASS OF COMPONENTS

Parameter	l_1	l_2	l_3	l_4	l_5	gb_2	gb_3	f_1
Length (mm)	7	30	13	12	17	30	30	35
Mass (g)	0.05	0.16	0.07	0.07	0.08			

1) Sub-chain 1 ($l_1 to\ l_2$)

$$K_1 = \frac{1}{2}[\dot{q}]^T\{m_1 \cdot [J_{v1}]^T[J_{v1}] + m_2 \cdot [J_{v2}]^T[J_{v2}]\}[\dot{q}] + \frac{1}{2}[\dot{q}]^T\left\{I_1 \cdot \begin{bmatrix}1 & 0\\ 0 & 0\end{bmatrix} + I_2 \cdot \begin{bmatrix}1 & 1\\ 1 & 1\end{bmatrix}\right\}[\dot{q}] \quad (10)$$

$$V_1 = m_1 g l_{1c}\sin(q_1) + m_2 g[l_1\sin(q_1) + l_{2c}\sin(q_1 + q_2)] \quad (11)$$

Where, $[\dot{q}] = \begin{bmatrix}\dot{q_1}\\ \dot{q_2}\end{bmatrix}, [J_{v1}] = \begin{bmatrix}-l_{c1}\sin(q_1) & 0\\ l_{c1}\cos(q_1) & 0\\ 0 & 0\end{bmatrix},$ (12)

$$[J_{v2}] = \begin{bmatrix}-l_1\sin(q_1) - l_{c2}\sin(q_1+q_2) & -l_{c2}\sin(q_1+q_2)\\ l_1\cos(q_1) + l_{c2}\cos(q_1+q_2) & l_{c2}\cos(q_1+q_2)\\ 0 & 0\end{bmatrix} \quad (13)$$

2) Sub-chain 2 ($l_3\ to\ l_4$)

$$K_2 = \frac{1}{2}m_{3+4}(l_{c3+c4}\dot{q_3})^2 + \frac{1}{2}I_{3+4}\dot{q_3}^2 \quad (14)$$

$$V_2 = m_{3+4}g l_{c3+c4}\sin(q_3) \quad (15)$$

3) Sub-chain 3 ($l_5\ to\ l_6$)

$$K_3 = \frac{1}{2}m_{5+6}(l_{c5+c6}\dot{q_4})^2 + \frac{1}{2}I_{5+6}\dot{q_4}^2 \quad (16)$$

$$V_3 = m_{5+6}g l_{c5+c6}\sin(q_4) \quad (17)$$

Lagrangian for each sub-chain is $L_i = K_i - V_i (i = 1,2,3)$ and for the entire system is the sum of sub-chain's Lagrangian.

$$L_{total} = \sum L_i \quad (18)$$

Assuming the device is inertially fixed with a constant pitch angle θ_a with respect to the ground, the equation of motion is

$$D(q_1)\ddot{q_1} + C(q_1, \dot{q_1})\dot{q_1} + G(q_1) = \tau_{motor} \quad (19)$$

III. AERODYNAMICS

In this section, quasi-steady aerodynamic model of a wing based on Blade Element Theory (BET) is addressed. Based on aerodynamic models presented by DeLaurier [9], Ellington [10] and Sane/Dickinson [12], some of unsteady effects were also taken into account in the model. In order to minimize the unsteady aerodynamic effects in the aerodynamic model, a Penaud-type FWMAV with stiff leading edge spar wing, flying at a constant pitch angle was considered. Since our focus was on the forward flight aerodynamics under Reynolds number for small birds ($Re \ll 10^5$), parameters such as flight speed, flapping frequency, dynamically varying pitch angle were selected in such a way that it doesn't exceed attached flow range of flapping flight and promotes negligible separated flow. The dynamically scaled model of a wing from [13] was also designed during this process, which employs EH2.0/10 airfoil with 2 % of camber with 10.07 % thickness. The wing was divided into a finite number of strips and incorporated into the aerodynamic model, which was adopted from [9-12]. Some approximations were directly employed from other literatures for convenience: C_{df} from [14], V_x from [10], Re from [15]. Not all the derivations of aerodynamic parameters will be presented in this section as it is beyond the main scope of this study. Hence, we begin from the point where we have obtained the section's normal (dN) and chord-wise (dF) force expressions.

Once dN and dF are obtained, section's lift (dL) and thrust (dT) can be computed as follow:

$$dL = dN\cos\theta_t + dF\sin\theta_t \quad (20)$$

$$dT = dF\cos\theta_t - dN\sin\theta_t \quad (21)$$

where $\theta_t = \theta_a + \theta_w + \delta\theta$. By integrating above two expressions over the semi-span of the wing gives instantaneous lift and thrust of a whole wing (right-side only).

$$L_r = \int_0^{\frac{b}{2}}\cos(q_4)\,dL = \int_0^{\frac{b}{2}}cos(q_4)(dN\cos\theta_t + dF\sin\theta_t)dy \quad (22)$$

$$T_r = \int_0^{\frac{b}{2}}dT = \int_0^{\frac{b}{2}}(dF\cos\theta_t - dN\sin\theta_t)\,dy \quad (23)$$

Also, average lift and thrust generation for one full cycle can be computed by integrating L_r, T_r over one full rotation of crank and divide by 2π. Given frequency, lift and thrust as a function of time ($L_{r_{(t)}}, T_{r_{(t)}}$) for one full cycle can also be computed,

$$L_{r_{ave}} = \frac{1}{2\pi}\int_0^{2\pi}L_r dq_1, \qquad T_{r_{ave}} = \frac{1}{2\pi}\int_0^{2\pi}T_r dq_1 \quad (24)$$

$$L_{r_{(t)}} = \frac{1}{2\pi}\int_0^{\frac{1}{f}}L_r dt, \qquad T_{r_{(t)}} = \frac{1}{2\pi}\int_0^{\frac{1}{f}}T_r dt \quad (25)$$

The section's aerodynamic moment about the flapping axis generated from the wing is,

$$dM_r = \{dN \cdot \cos(\theta_t - \theta_a) + dF \cdot \sin(\theta_t - \theta_a)\}dr_i \quad (26)$$

$$M_r = \int_0^{\frac{b}{2}}dM_r dy, \qquad M_{r_{ave}} = \frac{1}{2\pi}\int_0^{2\pi}M_r dq_1 \quad (27)$$

M_r is an instantaneous aerodynamic moment of the whole wing about the flapping axis, and $M_{r_{ave}}$ is an average aerodynamic moment during one cycle. The aerodynamic moment about the center of crank (M_{r_crank}) due to the forces from the right wing is

$$M_{r_{crank}} = M_r\frac{\dot{q_4}}{\dot{q_1}} \quad (28)$$

The same procedure can also be applied to derive the left wing's aerodynamic force and moment expressions. Then the total aerodynamic torque required from the motor is

$$\tau_{aero} = M_{r_{crank}} + M_{l_{crank}} \quad (29)$$

The equation of motion including aerodynamic model becomes

$$D(q_1)\ddot{q_1} + C(q_1, \dot{q_1})\dot{q_1} + G(q_1) = \tau_{motor} - \tau_{aero} \quad (30)$$

IV. ANALYSIS

A. Simulation criterion

Aerodynamic constants used in the simulation are given in Table. II. The orientation of vehicle coordinate frame is shown in Fig. 6. Often times we may call x-axis the longitudinal axis, y-axis the lateral axis and the z-axis the vertical axis. Common terminologies which will be used in later sections are; roll moment(M_x), yaw moment (M_z) and pitch moment (M_y). The simulation results shown in Fig. 7 are each wing's output angle displacement and velocity, lift, thrust, roll moment and aerodynamic torque required from the motor for one full flapping cycle. Three configurations of a system were simulated; gearbox positioned at the center ($c = 0$), gearbox shifted to the right ($c = +5$) and shifted to the left ($c = -5$). The x-axis used in all plots is a crank input (q_1) in degrees during one full cycle (90° to 450°). Note that the crank angle starts from 90° to 450° such that start and end of x-axis corresponds to the beginning of down stroke to the end of upstroke.

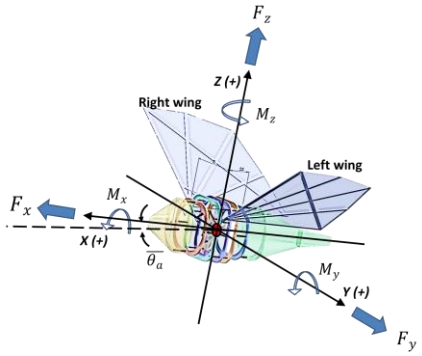

Figure 6. Vehicle coordinate frame and force/torque representation

Hereafter, a few notations will be used for convenience; i) symbol Φ denotes the peak to peak flapping wing amplitude, Φ_r for the right wing and Φ_l for the left wing, respectively, ii) c_0, c_{+5}, c_{-5} denotes three configurations of a system where c denotes the lateral shifting distance of the gearbox and the subscript number denotes a shifting value in *mm*. In other words, c_0 denotes when gearbox is at the center at which the flapping motion of two wings is exactly symmetric and in-phase ($\Phi_r = \Phi_l$). c_{+5} and c_{-5} denotes when gearbox is shifted either to the right ($\Phi_l < \Phi_r$) or to the left ($\Phi_l > \Phi_r$), respectively, at which asymmetric in-phase flapping motion of the wings occur.

TABLE II. AERODYNAMIC CONSTANTS

U	θ_a	β_0	f	ρ	v
5	4	0.01	4	1.225	$15.68 \cdot 10^{-6}$

B. Simulation results

Figure 7 (a)~(c): wing angle output displacements (q_4 , q_7) and velocity ($\dot{q}_4$, $\dot{q}_7$) from three configurations. The plots verify the performance of AIFM. We see changes only in amplitudes but have in-phase motion between the wings. (d)~(f): the peaks of lift curves are biased due to the change in Φ and also the sum of lift over the cycle becomes higher for the wing with lager Φ. But the total lift, (i.e., sum of lift of two wings) was equivalent to that of c_0 configuration. Hence, the net lift was consistent regardless of c. (g)~(i): there is a net positive thrust from all configurations. Higher net thrust was generated from the wing with larger Φ, as expected. Interestingly, the total thrust in c_{+5} and c_{-5} was higher than that of c_0. (j)~(l): In c_0, the net aerodynamic moment about the longitudinal axis is zero as the moment generated from each wing had the same magnitude but in opposite direction. In c_{+5} and c_{-5} cases, the magnitude of moment generated from each wing is no longer the same as the lift generation from each wing is different, which results in either positive or negative net roll moment. (m)~(o): the peak of required motor torque to generate a flapping motion was higher for larger Φ and lower for smaller Φ. Also, the total motor torque required in asymmetric in-phase flapping was higher than that of symmetric flapping.

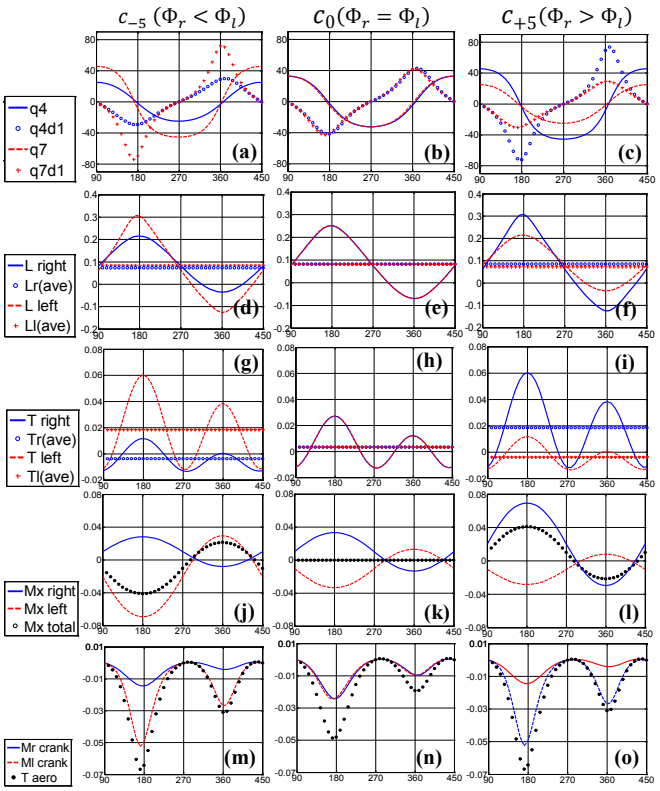

Figure 7. Simulation results under three configurations of gearbox position; c_{+5}, c_0, c_{-5}. The x-axis is in degree, y-axis is in *N* (force) or *N-m* (moment).

C. Experimental apparatus

A scaled model of AIFM (7.5 x 7.5 x 4.0 *cm*) was designed and fabricated using carbon fiber materials. The total mass was 8.3 grams including micro brushless motor and linear actuator. Then FWMAV was fabricated using AIFM, implementing electronic components that were remotely controlled (Fig 8). The total weight was 15 grams including the battery. Experimental test-bed was also designed and fabricated for conducting force measurements of three configurations (i.e., c_0 , c_{+5}, c_{-5}). A 6-axis force-torque sensor (NANO17) was mounted directly at the center of mass

location of the vehicle. All six components of force/torque generation was measured for last 10 seconds (fs = 2 kHz) during 1 minute of actuation, low-pass filtered (Butterworth 4th order, fl = 10 Hz), and averaged over one full cycle. The force measured from the sensors includes not only the aerodynamic forces from the wings but also the inertia forces of the mechanism itself. In this sense, additional experiment was carried out without the wings attached to the vehicle, then subtracted from the force measured with wings attached such that the errors from inertia force and mechanical vibration from the device can be canceled out in data analysis.

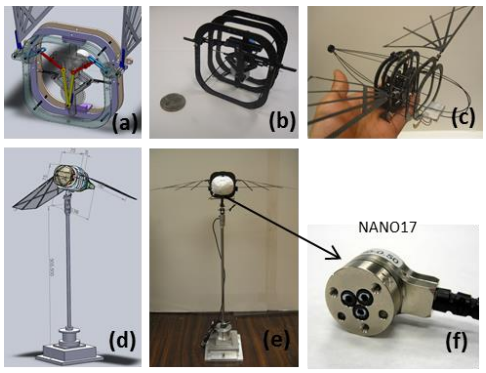

Figure 8. CAD of AIFM (a), AIFM fabrication (b), FWMAV fabrication (c), CAD of test-bed (d), Test-bed setup (e), NANO17 force/torque sensor (f)

D. Experiment results

The parameters used in simulation cannot be directly applied to the experimental study as the flight speed is zero in experimental environment. Hence, data shown in Fig. 9 should be only discussed for relative changes in forces and torques generated by AIFM and may not be used for direct comparison with simulation results. Nevertheless, some of experimental results still show a good agreement with simulation results. F_x (thrust) and F_z (lift) curves, for example, showed similar trend with simulation for c_{-5}, c_0, c_{+5}. Moderate increment in net lift and thrust was also observed from $c_{\mp 5}$ as compare to c_0 (Table. III). F_y (lateral force) of c_0 showed noticeable variation during one full cycle. It may be due to a little asymmetry about the longitudinal axis incurred during fabrication and that may have resulted in dynamic imbalance of the gearbox, thereby increasing the lateral vibration. In order to identify the relative changes in F_y between $c_{\mp 5}$ and c_0, $c_{\mp 5}$ values were subtracted from that of c_0 to obtain F_{y_rel}. It was observed that $c_{\mp 5}$ yield either positive or negative non-zero lateral force. M_{x_rel} and M_{z_rel} were computed in a same manner as F_{y_rel}. M_{x_rel} curves well matched the simulation results. Moreover, the net M_{x_rel} was non-zero which again verifies non-zero roll moment induced from asymmetric in-phase flapping motion. On the other hand, M_{z_rel} clearly showed a noticeable variation between c_{-5} and c_{+5}. Furthermore, M_z generated from c_{+5} and c_{-5} had the same magnitude but in opposite direction which clearly shows yaw moment was generated from asymmetric flapping. M_y showed slight increase from both of $c_{\mp 5}$ cases as compare to c_0.

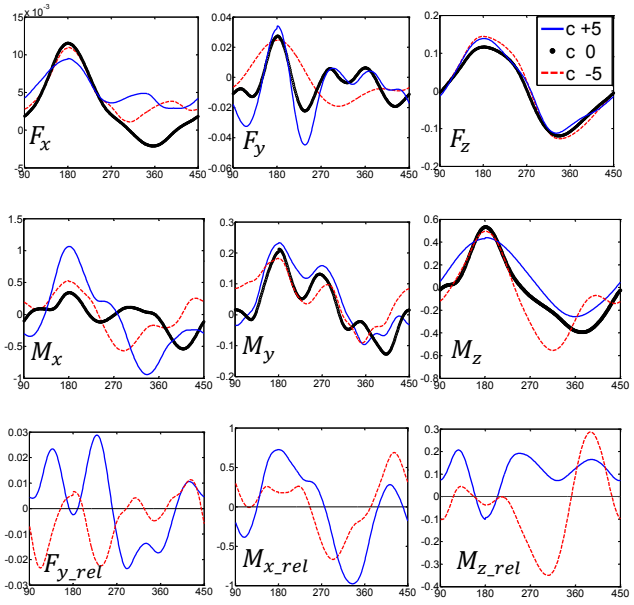

Figure 9. Experiment results showing force and torque generations from the AIFM-MAV. The x-axis is in degrees, y-axis is in *N* (force) or *N-m* (moment).

TABLE III. NET FORCE (N) & TORQUE(N-M) VALUES

c	F_x	F_y	F_z	M_x	M_y	M_z
-5	0.0047	0.0012	0.0043	0.0056	0.5628	-0.0640
0	0.0033	0.0032	0.0038	-0.3518	0.2909	0.0094
5	0.0053	0.0070	0.0039	-0.6222	0.5483	0.0657

V. DISCUSSION

The total lift generation was marginally consistent between symmetric and asymmetric flapping motion from both simulation and experiment results. This is due to the fact that the gain in lift from one side of the wing having larger amplitude is compensated by equivalent loss in lift from other side of the wing having smaller amplitude.

The total thrust was increased in asymmetric flapping from both simulation and experiment results. Asymmetric flapping motion induced a significant variation in thrust generation between two wings from simulation which can be directly correlated to the net yaw moment observed from the experiment.

The roll moment was zero throughout the full flapping cycle in symmetric flapping and net positive or negative roll moment generated from asymmetric flapping from simulation result. This result was well verified in the experiment which showed similar moment curves as well as comparable changes in net moment generation. It is also in accordance with other reports [5-8] which showed roll moment attained from differentiating lift generation of the two wings. The lateral shift of the center of mass due to change in gearbox position associated with asymmetric flapping motion actuation seemed not to influence the rolling dynamics of the system. The mass shifting (±5mm) was less than 7% of body width (75mm), and presumably the effect comes from change in inertia about the longitudinal axis of the body is negligible

compare to significantly higher aerodynamic forces dominating the overall dynamics of the system.

The total torque required from the motor due to the aerodynamic moments of wing was increased in asymmetric flapping from simulation. This is due to the increased net aerodynamic moment of the wings. Experiment results also verified that the device required higher power to reach 3.5 Hz to perform an asymmetric flapping,

The lateral force (F_y) was not being considered in the aerodynamic model as we assumed the spanwise flow is negligible by having higher wing aspect ratio undergoing attached steady flow. In general, lateral force is not emphasized in most of forward flight dynamic studies due to the same reason. Moreover, it can be assumed that net lateral force is zero if two wings have aerodynamic symmetry about the longitudinal axis, exerting equal but opposite lateral force about the longitudinal axis. However, as evidenced in our experiment, asymmetric in-phase flapping motion generated non-zero lateral force under no airflow condition. This finding may explain how some hovering insects can fly sideways. However, it should be interpreted with caution. The presence of net lateral force from asymmetric in-phase flapping may only be valid for very low speed inclined flight or hovering flight where airflow is more normal to the airfoil such that the spanwise flow can be present. As there is no theoretical explanation to validate our hypothesis any further, conclusive remark on lateral force generation will not be drawn here and will remain for the future studies.

Overall results on the dynamic effects induced from asymmetrically modulating flapping amplitude while keeping in-phase feature seems to be in good agreement with findings from the literatures [9-12]. However, there are some limitations in this study as well as some from the mechanism perspective that needs to be pointed out.

First and foremost, the important aspect of wing rotation in flapping flight has not been accounted for in this study. Although it was our intention to minimize the unsteady effects by disregarding the wing rotation in the aerodynamic model, it should be included in our follow up study to identify the combined dynamic effects of AIFM associated with wing rotation. Secondly, since present study only addresses the dynamics in forward flight condition with fixed angle of attack, inclined and hovering flight cases should be also explored. Thirdly, in order to fully characterize the attributes of this mechanism under various flight regimes, the system should be further analyzed in range of Reynolds number by using various f, Φ, U values and/or changing wing design parameters. Also, studies on 6 degree-of-freedom flight with asymmetric in-phase flapping should be followed as current results are only applicable to the body inertially fixed with respect to the ground. The argument on the net positive lateral force generation from AIFM must be carefully studied by looking at the spanwise flow during inclined or hovering flight, while also considering effects that come from vortices, wake and separated flow.

From the mechanism point of view, shifting the center of mass is coupled with asymmetric flapping motion. This has to be accounted for when we study 6 degree-of-freedom flight. Moreover, the maximum flapping amplitude of current design is less than 60 degrees where insects usually exhibit much higher flapping amplitude($\Phi \gg 90$). Therefore, next version of AIFM has to be designed that incorporates larger flapping amplitude and decouples the mass shifting to asymmetric flapping motion generation.

VI. Conclusion

This study was motivated from asymmetric flapping technique, often can be seen from nature's flyers, to generate a body torque required for maneuver and stabilization. The dynamic effects of asymmetric in-phase flapping motion in forward flapping flight was investigated by theoretical modeling of a mechanism, aerodynamic modeling of wings, fabrication of AIFM and FWMAV and analysis through simulation and experiment. Both simulation and experiment results showed comparable results in dynamic effects induced by AIFM. This mechanism was implemented into smaller scale FWMAV which showed its practical feasibility and potential to enhance current FWMAV performance. This study is also anticipated to help in better understanding of asymmetric in-phase flapping motion in flight dynamic controls and further provides a physical tool to integrate other wing motion attributes, such as asymmetric wing rotation and asymmetric stroke plane control.

References

[1] J. Park, E.P. Yang, C. Zhang, and S.K. Agrawal, "Kinematic design of an asymmetric in-phase flapping mechanism for MAVs," *Robotics and Automation, ICRA 2012. IEEE International Conference on* , vol., no., pp.5099-5104, 2012

[2] R. Dudley, "The biomechanics of insect flight- form, function and evolution," *Princeton University Press*, 2000

[3] M. Sun and X. Yan, "Dynamic flight stability of a hovering bumblebee", *J Exp Biol*, Vol. 208, 447-459, 2005

[4] M. Dickinson and M. Tu, "The function of dipteran flight muscle," *Comp. Biochem. Physiol*., vol. 116A, no. 3, pp. 223–238, 1997.

[5] T. Hedrick, B. Cheng, and X. Deng, "Wingbeat Time and the Scaling of Passive Rotational Damping in Flapping Flight, *Science* 324, 252-255, 2009

[6] T. Hedrick, "Damping in flapping flight and its implications for manoeuvring, scaling and evolution", *J Exp Biol* 214, 4073-4081, 2011

[7] B. Finio, J.K. Shang, and R.J. Wood, "Body torque modulation for a microrobotic fly," *Robotics and Automation, 2009. ICRA '09. IEEE International Conference on* , vol., no., pp.3449-3456, 2009

[8] B. Finio, B. Eum, C. Oland, and R.J. Wood, "Asymmetric flapping for a robotic fly using a hybrid power-control actuator," *Intelligent Robots and Systems, 2009. IROS 2009. IEEE/RSJ International Conference on* , vol., no., pp.2755-2762, 2009

[9] J.D. DeLaurier "An Aerodynamic Model For Flapping-Wing Flight," *Aeronaut. J*., Vol. 97, No. 964, 125-130,1993

[10] J.D. DeLaurier, "An Ornithopter Wing Design," *Can. Aero. Space J*., Vol. 40, No. 1, 10-18, 1994

[11] C.P. Ellington, "The novel aerodynamics of insect flight- Applications to micro-air vehicles," *J. exp. Biol*., B 202, 3439-3448, 1999

[12] S.P. Sane, and M.H. Dickinson, "The aerodynamic effects of wing rotation and a revised quasi-steady model of flapping flight," *J. exp. Biol*., 205, 1087–1096, 2002

[13] J. Park, and K. Yoon, "Designing Cicada-Mimetic Flapping Wing with Composite Wing Structure and Application to Flapping MAV," *Studies in Computational Intelligence: Intel. Unmanned Systems,* Vol. 192, pp. 119 – 133, 2009

[14] S.F. Hoerner, "Skin-friction drag, Fluid-Dynamic Drag," Published by the Author, Brick Town, NJ, pp 2-1 to 2-16, 1965

[15] J.R. Usherwood, C.P. Ellington "The aerodynamics of revolving wings. I. Model hawkmoth wings," *J. exp. Biol*., 205, 1547-1564, 2002